Med Biol Eng Comput (2012) 50:1163–1172
DOI 10.1007/s11517-012-0921-9

SPECIAL ISSUE - ORIGINAL ARTICLE

A novel EDA glove based on textile-integrated electrodes for affective computing

Antonio Lanatà · Gaetano Valenza · Enzo Pasquale Scilingo

Received: 26 July 2011 / Accepted: 21 May 2012 / Published online: 19 June 2012

Abstract This paper reports on performance evaluation of a preliminary system prototype based on a fabric glove, with integrated textile electrodes placed at the fingertips, able to acquire and process the electrodermal response (EDR) to discriminate affective states. First, textile electrodes have been characterized in terms of voltage–current characteristics and trans-surface electric impedance. Next, signal quality of EDR acquired simultaneously from textile and standard electrodes was comparatively evaluated. Finally, a dedicated experiment in which 35 subjects were enrolled, aiming at discriminating different affective states using only EDR was designed and realized. A new set of features extracted from non-linear methods were used, improving remarkably successful recognition rates. Results are, indeed, very satisfactory and promising in the field of affective computing.

Keywords Electrodermal response · Textile electrode · Affective computing · Biomedical signal processing

1 Introduction

In the last century, emotions (i.e., identification and recognition) have become one of the most noteworthy research areas. Recent studies have shown that concepts like human feelings and mood, and the way which humans perceive the environment and the others are very interwoven in all human activities, mental states, hilliness, etc. [6, 32]. Even though emotion identification still remains one of the most controversial concepts to be univocally defined, many models of emotion have been proposed [14, 33]. However, these emotional models have allowed researchers to develop systems that try, more or less automatically, to recognize the affective states by interpreting physiological correlate changes following to an external event. Recently, several engineering approaches have been used to guarantee acceptable emotion recognition, along with high accuracy, robustness, and adaptability to practical applications. An emotion recognition system is generally composed of two main parts: emotion elicitation and physiological correlate identification. The first part, which is very crucial, could be performed through different perceptual channels, such as audio, visual (image or video) [13, 19, 38], or using personalized imagery stimuli, [30]. The difficulty associated to the elicitation is related to a complex interaction between cognition and neurophysiological changes. Circumplex theorists conceptualize the elicitation of a strong emotion as a neurophysiological state typically involving the combination of a positive/negative valence and intense arousal in the central nervous system (CNS) [32]. This theoretical concept involves the emotional experience, which is a cognitive interpretation of physiological patterns in the context of eliciting stimuli. Emotions can therefore be seen as a result of this complex interaction. In many works, the international affective picture system (IAPS) photoset [21] is used to elicit target emotions with variable levels of valence and arousal and results are widely adopted for psychophysiological studies. The idea behind the second part of the system is that

A. Lanatà · G. Valenza · E. P. Scilingo (✉)
Faculty of Engineering, Interdepartmental Research Centre "E. Piaggio", University of Pisa, Via Diotisalvi, 2, 56126 Pisa, Italy
e-mail: e.scilingo@ing.unipi.it;
e.scilingo@centropiaggio.unipi.it

A. Lanatà
e-mail: alanata@centropiaggio.unipi.it

G. Valenza
e-mail: g.valenza@iet.unipi.it

autonomic nervous system (ANS) reflects measurable changes according to emotional experience [26, 32]. In detail, many researchers have observed that peripheral physiological responses to affective stimuli vary incrementally with subjective ratings of valence and arousal. In addition, many investigators have correlated skin conductance and heart rate variation with subjective ratings of arousal [34, 37]. Since the electrodermal responses (EDR) have been shown to be a powerful signal emotion related [37], this work aims at investigating the acquisition of EDR by means of a comfortable glove which incorporates textile electrodes. Moreover, a dedicated affective computing experiment was performed, whose results are reported in terms of capability of discriminating different levels of arousal.

2 Methods

2.1 The electrodermal response

The EDR represents changes in the skin electrical properties, i.e., electric impedance, due to psychologically induced sweat gland activity [39] upon an external stimulus. More specifically, it is strictly related to the activity of the eccrine sweat glands (located in the palms of the hands and soles of the feet) and the skin pore size. In a variety of induction contexts, electrodermal reactivity consistently varies with emotional intensity. Many studies have found that skin conductance increases when people view pictures rated as emotional, compared to neutral, regardless of whether they are rated pleasant or unpleasant [22, 24, 39]. Moreover, when listening to affective sounds [1], or music [12], skin conductance activity increases as the acoustic stimuli are highly rated in emotional arousal. Elevated electrodermal reactions are also found when people watch film clips classified as pleasant or unpleasant [4]. The scientific community has accepted to consider the EDR as indirect indicator of the sympathetic nervous system [37]. Several approaches are used to measure this signal. In this work, a small continuous voltage, of 0.5 V, is applied to the skin and the induced current is measured through two electrodes positioned at the index and middle fingertips of the non-dominant hand. The use of continuous or alternating voltage as voltage source in the EDR measurement is still a controversial issue, even though the first method allows avoiding possible electrode polarization and skin electrolysis. As there is no agreement in the literature on this point, we decided to follow the recommendations provided by Ref. [10], where an acceptable methodology for recording the electrodermal activity, reflecting a wide consensus of experts in the field, is proposed.

The ratio between voltage drop and induced current represents the skin electric impedance. Electrodermal response changes depend on the individual physiological state as well as on interaction with environmental events. The EDR can be split into two components: tonic and phasic. Tonic component is the baseline level of skin conductance (also called skin conductance level—SCL), whose trend is different from person to person and depends on both physiological state and autonomic regulation. Phasic component (also called skin conductance responses—SCRs), superimposed on the tonic baseline level, changes with specific external stimuli such as lights, sounds, smells, etc. or events. In this paper, we focused on identifying changes in EDR through a textile-based sensing glove upon emotional stimuli. The use of a wearable textile system exhibits several advantages in terms of portability and usability for long-term monitoring, and gives minimal constraints.

2.2 The glove system

In this work a preliminary system prototype consisting of a fabric glove, whose textile substrate is lycra, with integrated textile electrodes placed at the fingertips, and a dedicated electronic card including an analog front-end, a

Fig. 1 Fabric glove including textile electrodes connected to a dedicated electronic card

digital block, and a wireless real-time communication module for data transmission to a remote personal computer (PC), (see Fig. 1) was developed. Due to manufacturing reasons, the fabric glove incorporates textile electrodes at level of the first four fingers, although only the first two have been used for the experimental session. This choice was made according to guidelines reported in Ref. [10]. The analog front-end consists of a DC voltage source, a Wheatstone bridge followed by a set of filters and amplifiers. Fig. 1.

2.3 Textile electrode performance assessment

Textile electrodes were first characterized identifying the current–voltage curve and evaluating the electrode impedance in terms of magnitude and phase in the bandwidth of the EDR. Afterwards, they were used together with standard electrodes Ag/AgCl in order to acquire simultaneously EDRs from them and make a quantitative comparison.

2.3.1 Textile electrode characterization

A suitable electrochemical cell was realized to characterize textile electrodes (see Fig. 2a). It is composed of a textile and a reference electrode immersed into a solution of potassium chloride (KCl) 0.1 M. The electrodes are placed at a distance of 3 mm, immersed into 0.015 l of solution, and connected to an external measurement device.

Textile electrodes were provided by Smartex s.r.l., and have been already described in literature [7, 36]. They are made up of 80 % polyester yarn knitted with 20 % steel wire, with a dimension of 1 × 1 cm (see Fig. 2b). The reference electrode is represented by a standard platinum electrode of 3 × 4 cm (see Fig. 2c). The reference electrode size was chosen to be larger than the textile electrode to minimize border effects.

2.3.1.1 Current–voltage characteristics identification The current–voltage characteristics were identified by applying a varying source voltage and determining the current flowing through the cell. This measurement is performed with the aim of investigating the electrode reaction due a differential potential applied between sensing and reference electrodes. In particular, an offset-free voltage varied from 1 to 20 peak-to-peak volts, with an increasing step of 1.2 V, at frequency of 0.1 Hz, has been applied. Experimental measurements were fitted using the Butler–Volmer equation, which is defined as:

$$j = j_0\left(e^{\alpha\frac{zF}{RT}\eta} - e^{-(1-\alpha)\frac{zF}{RT}\eta}\right) \quad (1)$$

where j is the electrode density current (A m^2), j_0 is the exchange density current (A m^2), η is the over-potential (Volt), T is the absolute temperature (K), F is the Faraday constant, R is the universal gas constant, z is the valence of the ion, and α is the transfer coefficient. By analogy with Ohm Law ($V = IR$) and for small overpotentials the gradient of the relation between η and j can be interpreted as the equivalent resistance per unit area of the charge-transfer process on the electrode and is called the charge transfer resistance R_T [31]. R_T can be obtained as:

$$R_T = \frac{\partial\eta}{\partial j} = \frac{TR}{\alpha z F j_0} \quad (2)$$

To evaluate the agreement of our experimental measurements with the Butler–Volmer equation, a non-linear least square fitting method was used. The goodness of fit was evaluated by calculating the well-known statistic index *Adjusted R-square*.

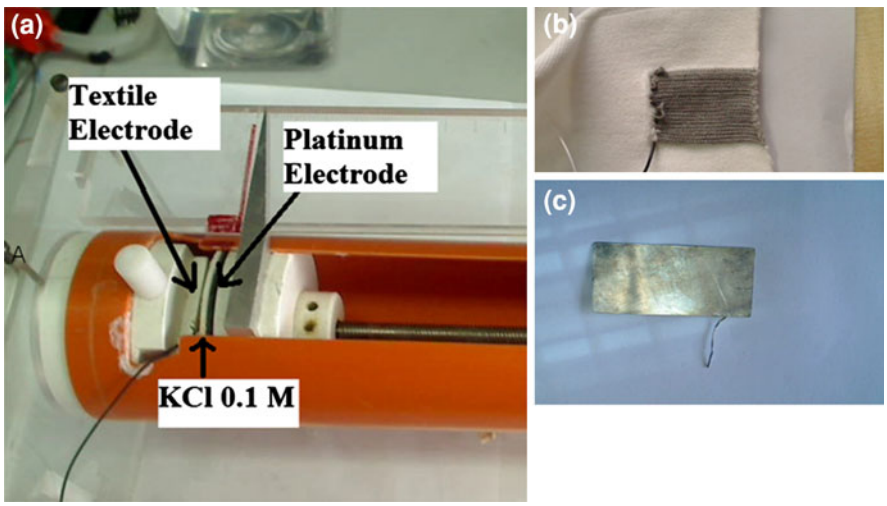

Fig. 2 Electrolytic cell (**a**), textile electrode (**b**), platinum reference electrode (**c**)

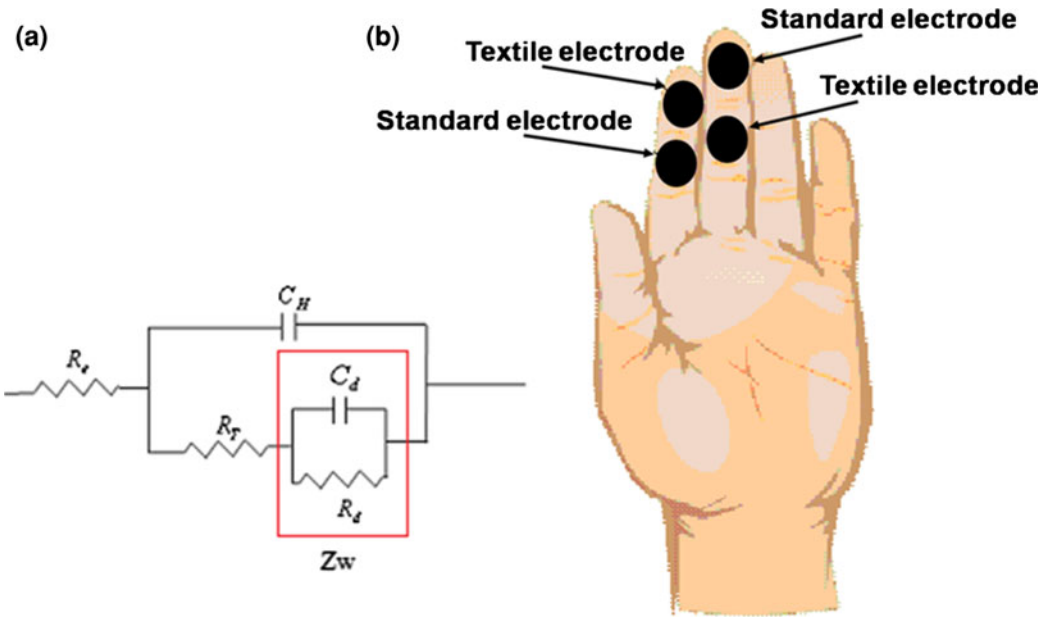

Fig. 3 Equivalent electric model of electrode (**a**), electrode placement in crossed configuration (**b**)

2.3.1.2 Surface electric impedance evaluation The electrode was also characterized by estimating the trans-surface electric impedance. This measurement is used to investigate how the phase and amplitude of the electrode impedance change in the frequency domain. The impedance of electrodes in ionic liquids has been currently investigated experimentally and theoretically [15]. Figure 3a shows an equivalent circuit that models the relevant phenomena. In our experimental characterization, the same electrochemical cell is used with the same solution. The amplitude of the voltage applied between the electrodes was fixed while its frequency was varied in the range of the EDR bandwidth (from 0.01 to 2.1 Hz with a step of about 0.13 Hz). In this equivalent circuit, C_H is the interface capacitance per area unit, which consists of the series combination of the Helmholtz double layer and the diffuse layer where Z_w is the Warburg impedance, R_T is the charge-transfer resistance and R_e is the spreading resistance. The Warburg impedance is reported as follows:

$$Z_w = \frac{\omega^{-\frac{1}{2}}}{A}\frac{k}{1+j} \tag{3}$$

where A is the electrode area and $k\left[\Omega s^{-\frac{1}{2}}cm^2\right]$ is constant. The low frequency of EDRs implies, according to previous works [28], that both Warburg and interface capacitance terms are important for this characterization.

All the experiments were carried out at 25 °C and pressure of 1 atm.

2.3.2 Textile-based EDR validation

Textile-based EDR was further validated by simultaneously acquiring EDR through textile and standard Ag/AgCl electrodes. Both signals were acquired using the MP35 Biopac system with a sampling frequency of 1 kHz.

It was found in the literature that skin conductance activity is greater at distal than medial site of fingers, and is attributable to a greater number of active (open) sweat glands at distal sites [11]. To minimize artifacts due to the different concentrations of sweat glands at the distal and medial sites, we placed electrodes in a crossed configuration, as shown in Fig. 3b. Both the signals were filtered with a 2.5 Hz low-pass finite impulse response filter approximated by a Butterworth polynomial. To consider only the variation of both textile and standard EDRs, data were normalized to the maximum value. The comparison was performed by means of a non-parametric coefficient, Spearman correlation [12], due to non-gaussianity of EDR signals. Moreover, a ten-level wavelet decomposition was applied to the EDR to obtain tonic and phasic signals using the Daubechies 5 function. The approximation at level 1 is tonic, and the details from levels 2 to 8 are phasic. We decided to apply wavelet decomposition, because it is a powerful tool for analyzing the components of a non-stationary signal. The Spearman correlation was calculated for both tonic and phasic signals.

2.4 Psycho-physiological evaluation: experimental setup

Data were acquired by means of the glove shown in Fig. 1 using only the index and middle fingers. The experimental setup is structured into the following phases: recruitment of eligible subjects, affective state elicitation, and acquisition and processing of the physiological signal set.

Table 1 Rating of IAPS images used in this work

Sess. session, *N.I* number of images, *N* neutral, *V* valence, *A* arousal, *A1* arousal 1, *A2* arousal 2, *A3* arousal 3, *A4* arousal 4

Sess.	N.I.	V. rating	V. range	A. rating	A. range
N	6	6.49 ± 0.87	5.52 ÷ 7.08	2.81 ± 0.24	2.42 ÷ 3.22
A1	20	/	2.87 ÷ 7.63	3.58 ± 0.30	3.08 ÷ 3.98
A2	20	/	1.95 ÷ 8.03	4.60 ± 0.31	4.00 ÷ 4.99
A3	20	/	1.78 ÷ 7.57	5.55 ± 0.28	5.01 ÷ 6.21
A4	20	/	1.49 ÷ 7.77	6.50 ± 0.33	5.78 ÷ 6.99

2.4.1 Recruitment of eligible subjects

A group of 35 healthy subjects, i.e., not suffering from evident mental pathologies, was recruited to participate in the experiment. Their age ranged from 21 to 24, and were naive to the purpose of the experiment.

2.4.2 Stimulation protocol

The affective elicitation is performed by projecting a set of images to a PC monitor. These images are chosen from the official IAPS database. In this work, the slideshow was projected in a properly room equipped with dedicated monitor and headset to acoustically insulate from external noise. The slideshow comprises nine sessions of images *N*, *A*1, *N*, *A*2, *N*, *A*3, *N*, *A*4, *N* where *N* is a session of six neutral images (mean valence rating 6.49, SE = 0.87, range = 5.52 ÷ 7.08; mean arousal rating = 2.81, SD = 0.24, range = 2.42 ÷ 3.22), and *Ai* (with *i* going from 1 to 4) are sets of 20 images eliciting increasing level of arousal. Detailed values are reported in Table 1. The overall protocol utilizes 110 images. Each image is presented for 10 s for a total duration of the experiment of 18 min and 20 s.

The EDR signal acquired during the IAPS elicitation is then segmented and filtered. Afterwards, the most significative features are extracted and classified using various machine-learning methods [17]. In particular, we tested several classifiers such as linear discriminant classifier (LDC), mixture of gaussian (MOG), *k*-nearest neighbor (*k*-NN), Kohonen sel- organizing map (KSOM), multilayer perceptron (MLP), and quadratic discriminant classifier (QDC). Among these, QDC has shown the highest recognition accuracy and consistency in both arousal and valence multiclass. According to that and for the sake of brevity we will report and discuss here only results from the QDC.

2.4.3 Signal acquisition and processing

In this work, all the features were calculated for each neutral session as well as for each A_i session. In this work we used two big categories of features: the most commonly used standard features, and features extracted from non-linear dynamic techniques. In detail, 41 standard features and 12 extracted from non-linear methods are used (see Table 2). In the literature, different definitions of the frequency ranges of tonic and phasic components can be found. While it is widely accepted that the tonic component is the background level changing very slowly and the phasic component varies with the external stimulus, the upper cut-off frequency of the tonic component is controversial. Here, we used a frequency bandwidth separation proposed in [16], and the signal was analyzed in following bands: 0–0.05 Hz, 0.05–1 Hz, and 1–2 Hz.

Table 2 The whole feature sets used as input to the classifier

Feature set	Analysis	Signals
Standard	Frequency domain (power in 0–0.1 Hz, 0.1–0.2 Hz, 0.2–0.3 Hz, 0.3–0.4 Hz, rate)	Phasic EDR
	Frequency domain (Rate)	Tonic EDR
	Statistics (SEM, Mean, SD, MFD, SDFD, MSD, SDSD skewness, kurtosis)	Tonic and Phasic EDR
	Statistics (max peak, latency, MAD, MDNV, PNSDAS)	Phasic EDR
	High-order spectra (MBI, VBI, MMB, PEB, NBE, NBSE)	Tonic and phasic EDR
Non-linear methods	Deterministic chaos (m, Δ)	Phasic EDR
	Recurrence plot (DLE, RR, DET, LAM, TT, RATIO, ENTR, L_{max})	Phasic EDR
	Detrended fluctuation analysis (α_1, α_2)	Phasic EDR

2.4.3.1 Feature extraction Several features, described in detail below, can be extracted from the EDR using standard and non-linear methods.

1. Standard feature set: Standard features are derived from time series, statistics, frequency domain, geometric analysis for the whole set of physiological signals. The whole signal was segmented in consecutive time windows *W*, in which a wide set of standard features, including mean and standard deviation of first (MFD and SDFD, respectively) and second derivative (MSD and SDSD, respectively), mean and standard deviation (SD) of the amplitude [22], standard error of the mean (SEM), were calculated.

Other higher-order statistical features, such as skewness and kurtosis, are calculated. In the frequency domain, *Rate* is calculated as the frequency corresponding to the maximum spectral magnitude. Some features are extracted only from the phasic component of EDR: maximum peak and the relative latency from the beginning of each image, mean of absolute of derivative (MAD), mean of derivative for negative values (MDNV), proportion of negative samples in the derivative versus all samples (PNSDAS). In the frequency domain, spectral power in the bandwidths 0–0.1 Hz, 0.1–0.2 Hz, 0.2–0.3 Hz, and 0.3–0.4 Hz are also calculated [20].

Standard features from higher-order spectra: In addition to the above-mentioned standard techniques, high-order spectra (HOS) is also examined, which is defined as Fourier transform of moments or cumulants of order greater than two. In particular, we used the two-dimensional third-order cumulant Fourier transform, called bispectrum [25, 27]:

$$B(f_1,f_2) = \iint_{t_1,t_2=-\infty}^{+\infty} c_3(t_1,t_2)\exp^{-j(2\pi f_1 t_1 + 2\pi f_2 t_2)}\mathrm{d}t_1\mathrm{d}t_2 \qquad (4)$$

with the condition: $|\omega_1|, |\omega_2| \leq \pi$ for $\omega = 2\pi f$

The $c_3(t_1, t_2)$ variable represents the third-order cumulant, which is defined as follows:

$$c_3(t_1,t_2) = E\{s(t_1)s(t_2)s(t_1+t_2)\} \qquad (5)$$

where $s(t)$ is a square integrable stationary signal with zero mean. Bispectrum, indeed, measures the correlation among three spectral peaks, ω_1, ω_2 and $(\omega_1 + \omega_2)$ and estimates the phase coupling. A previous study demonstrated that bispectrum has several symmetry properties [27] and divides the (f_1, f_2) plane in eight symmetric zones. Bispectrum of a real signal is uniquely defined by its values in the triangular region of computation, $0 \leq f_1 \leq f_2 \leq f_1 + f_2 \leq 1$, provided there is no bispectral aliasing [2]. The bispectral feature set consists of: mean and variance of bispectral invariants (MBI and VBI), i.e., mean and variance of $P(a)$, mean magnitude (M_{mean}) of bispectrum (MMB) and phase entropy P_e (PEB), normalized bispectral entropy P_1 (NBE) and normalized bispectral squared entropy P_2 (NBSE). All the features are calculated within the region defined by Chang et al. [3], and Chua et al. [5].

2. Non-linear dynamic methods for feature extraction: Here we propose a new set of features extracted from non-linear methods and applied to phasic components of the EDR signal. A powerful technique used for analysis of complex dynamical systems is the so-called embedding procedure. Embedding of a time series $x_t = (x_1, x_2,\ldots,x_N)$ is done by creating a set of vectors X_i such that

$$X_i = [x_i, x_{i+\Delta}, x_{i+2\Delta}, \ldots, x_{i+(m-1)\Delta}] \qquad (6)$$

where Δ is the delay in number of samples and m is the number of samples (dimension) of the array X_i. The number of samples in the embedded vector is usually chosen to be large enough to cover the dominant frequency in the time series, but m should not be so large that the first and last values in the epoch are practically unrelated. The evolution of the system can be now represented by the projection of the vectors X_i onto a trajectory through a multidimensional space, often referred to as phase space or state space. Moreover, recurrence plot (RP) [23] is a graph showing all the times at which a state of the dynamical system recurs, i.e., all the times the phase space trajectory visits roughly the same area in the phase space. Eckmann et al. [9] proposed a tool enabling to investigate the m-dimensional phase space trajectory through a two-dimensional representation of its recurrences. When a state at time i recurs also at time j, the element (i, j) of a squared matrix $N \times N$ is set to 1, 0 otherwise. Recurrence plot can be also represented according to this scheme and can be mathematically expressed as

$$R_{i,j} = \Theta\left(\varepsilon_i - ||x_i - x_j||\right)$$

where $x_i \varepsilon R^m$, $i.\ j = 1,\ldots N$; N is the number of considered states x_i, ε_i is a threshold distance, $||.||$ a norm and $\Theta(.)$ the Heaviside function which is defined as:

$$H(z) = \begin{cases} 1, & \text{if } z \geq 0 \\ 0, & \text{if } z < 0 \end{cases} \qquad (7)$$

In this work we chose the optimal value of ε_i [35] as:

$$\varepsilon_i = 0.1 \times A_{\text{PD}} \qquad (8)$$

where A_{PD} is averaged phase space diameter of data x_i.

Following the above description, the recurrence quantification analysis (RQA) [40] is a method of non-linear data analysis which quantifies the number and duration of recurrences of a dynamical system presented by its state space trajectory. Quantification of recurrence plots can be based either on evaluating diagonal lines to estimate chaos-order transitions or on vertical (horizontal) lines to estimate chaos–chaos transitions. In this work the following features are calculated: recurrence rate (RR), determinism (DET), laminarity (LAM), trapping time (TT), ratio (RATIO), averaged diagonal line length (L), entropy (ENTR), and longest diagonal line ($L_{\max}$). In stochastic processes, chaos theory and time series analysis, detrended fluctuation analysis (DFA) is a method for determining the statistical self-affinity of a signal. The DFA method has proven useful in revealing the extent of long-range correlations in time series [29]. In brief, the time series to be analyzed (with N samples) was first integrated, then divided into boxes of equal length n. In each box of length n, a least squares line fits the data (representing the trend in that box). The y coordinate of the straight line segments is denoted by $y_n(k)$. Next, we detrended the integrated time series, $y(k)$, by subtracting the local trend, $y_n(k)$, in each box. The root-

mean-square fluctuation of this integrated and detrended time series was calculated as

$$F(n) = \sqrt{\frac{1}{N}\sum_{k=1}^{N}[y(k) - y_n(k)]^2} \tag{9}$$

2.4.3.2 Feature reduction Since a large number of features are calculated, a reduction of the feature space dimension is necessary. We chose the widely used principal component analysis (PCA), which is able to project high-dimensional data to a lower dimensional space with a minimal loss of information [18].

2.4.3.3 Classification In this work results from QDC are shown. It is a parametric classifier based on Bayesian decision theory, and allowed us to minimize the overall risk, guaranteeing the lowest average error rate. After the training process, the performance of the classification task is commonly evaluated using the confusion matrix. The generic element r_{ij} of the confusion matrix indicates how many times in percentage a pattern belonging to the class i was classified as belonging to the class j. A more diagonal confusion matrix corresponds to a higher degree of classification. The matrix has to be read by columns. The training phase is carried out on 80 % of the feature dataset (subset from 28 subjects) while the testing phase to the remaining seven subjects. We performed 40-fold cross-validation steps in order to obtain unbiased classification results, i.e., it allowed us to consider the gaussian distribution of classification results, which can be therefore described as mean and standard deviation among the 40 confusion matrix obtained. Quadratic discriminant classifier [8] uses a supervised learning method which determines the parameters based on available knowledge. We assume that the input training data is a finite set $\Gamma\{(x_1,y_1),\ldots,(x_l,y_l)\}$ containing pairs of observations $x_i \in R^n$ and corresponding class labels $y_i \in Y$. Basically, statistical classifiers use *discriminant functions* $f_y(x)$, $\forall y \in Y = \{1,2,\ldots,c\}$ for c classes input dataset and x is a *d-component* feature vector. The classifier is said to assign a feature vector x to class y_i if:

$$f_i(x) > f_j(x) \quad \forall j \neq i \tag{10}$$

A Bayes-based classifier is viewed as a network or machine that computes c discriminant functions and selects the category corresponding to the largest discriminant. For the general case with risks, we can let $f_i(x) = -R(\alpha_i|x)$, since the maximum discriminant function will then correspond to the minimum conditional risk. For the minimum-error-rate case, we can take $f_i(x) = P(y_i|x)$, so that the maximum discriminant function corresponds to the maximum posterior probability. The effect of any decision rule is to divide the feature space into c decision regions, $\Re_1,\ldots,\Re_c$. If $f_i(x) > f_j(x)\,\forall j \neq i$, then x is in region $\Re_1$, and the decision rule assigns x to f_i. The regions are separated by decision boundaries, surfaces in feature space where ties occur among the largest discriminant functions. The structure of a Bayes classifier is determined by the conditional densities $P(x|y_i)$ as well as by the prior probabilities, according to the Bayes theorem:

$$P(y_i|x) = \frac{P(x|y_i)P(y_i)}{P(x)} \tag{11}$$

where $P(y_i)$ and $P(x)$ are the prior probabilities. Assuming that the minimum-error-rate classification can be achieved by using the discriminant functions [8]:

$$f_i(x) = lnP(x|y_i) + lnP(y_i) \tag{12}$$

If the densities $P(x|y_i)$ are multivariate normal, i.e. $P(x|y_i) : N(\mu_i, \Sigma_i)$ where μ_i is the *d-component* mean vector and Σ_i is the *d-by-d* covariance matrix, we obtain:

$$f_i(x) = -\frac{1}{2}(x-\mu_i)^t\Sigma_i^{-1}(x-\mu_i) - \frac{d}{2}ln2\pi - \frac{1}{2}ln|\Sigma_i| + lnP(y_i) \tag{13}$$

where $(x-\mu_i)^{\mathrm{t}}$ is the transpose of $(x-\mu_i)$ matrix. In the general multivariate normal case, the covariance matrices are different for each category. The only term that can be dropped from the above equation is the $\frac{d}{2}ln2\pi$ term, and the resulting discriminant functions are inherently quadratic with respect to the input vector $x \in R^n$:

$$f_y(x) = x^t \cdot A_y x + b_y x + c_y, \quad \forall y \in Y$$

The quadratic discriminant function f_y is determined by:

$$A_y = -\frac{1}{2}\Sigma_i^{-1} \tag{14}$$

$$b_y = \Sigma_i^{-1}\mu_i \tag{15}$$

$$c_y = -\frac{1}{2}\mu_i^t\Sigma_i^{-1}\mu_i - \frac{1}{2}ln|\Sigma_i| + lnP(y_i) \tag{16}$$

Of course, if the distributions are more complicated, the decision regions can be even more complex, though the same underlying theory holds there too.

3 Results

3.1 Results of the assessment of the textile electrode performance

The experimental results, of the textile electrode performance, are presented here for both textile electrode characterization and EDR evaluation. Figure 4 shows the experimental data fitting the Butler–Volmer equation, from

which α (transfer coefficient) was 3.022×10^{-2}, j_0 (exchange current density) was 3.639×10^{-4} A/m^2, and R_T (charge transfer resistance) was 2358.78 $\Omega \times$ m^2.

In addition, outside the region of validity of the Butler–Volmer equation, a limiting current density J_{SAT} was experimentally detected and resulted to be 0.0103 (A/m^2). The goodness of fit was about of 0.969, calculated by Adj(R2), which confirmed the good agreement between theoretical and experimental data. Figure 5 reports the magnitude (Fig. 5a) and phase (Fig. 5b) of the textile electrode impedance calculated in the frequency bandwidth of the EDR, where the impedance magnitude decreases as frequency increases and phase is pretty linear implying a constant group delay and no distortion introduction.

Spearman correlation coefficient was calculated between signals coming from standard and textile electrodes for tonic and phasic components of EDR as well as for the whole signal. Spearman correlation for tonic and phasic skin conductance were 0.957 ± 0.024 and 0.995 ± 0.001, respectively. In addition, the correlation for the whole EDRs in crossed-finger configuration was 0.960 ± 0.031. Although physical properties of the textile fibres used to realize the electrodes, e.g., diameter, number of fibers per unit of area, geometry, manufacturing methods (knitting, embroidery, and sewing) can affect the electrical performance a detailed study on that goes beyond the purpose of this manuscript. In our experiment we used textile electrodes made up of stainless steel based fibres and yarns. The yarns are produced by Schoeller, with a composition of 80 % polyester and 20 % stainless steel. A performance evaluation of this typology of textile electrodes has been carried out and results, as shown above, confirm that there is not relevant difference between textile and standard electrodes while measuring the electrodermal activity.

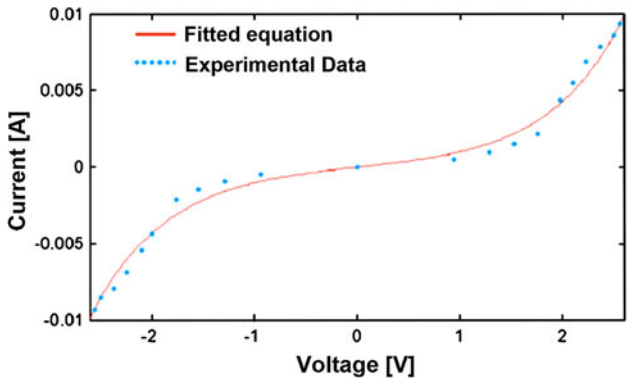

Fig. 4 Fitting of Bulter–Volmer equation

3.2 Results of the psycho-physiological evaluation

Experimental psycho-physiological evaluation results from the QDC are shown in Table 3 in the form of confusion matrix when using only standard features (α), only features extracted from non-linear methods (β), and when using both together (γ). It is obtained by the cross-validation technique, which is an average of 40 confusion matrix calculated on a randomly shuffled dataset. In each element constituting the diagonal it has been reported mean value and standard deviation of the classification result for that class, respectively. In all other elements the error of classification is reported as well. Each principal component, obtained from applying the PCA algorithm to the feature sets, accounts for a given amount of the total variance. We stopped the reduction process when the cumulative variance reached 95 %. Therefore, the number of principal components is different for standard dataset and the joint dataset (see caption of the table for further details).

4 Discussion

In this paper, we explored the possibility of using a fabric glove including textile electrodes to acquire EDR. Firstly, textile electrodes have been electrically characterized; then, they are used to acquire EDR in a dedicated affective computing experiment. More specifically, a set of features

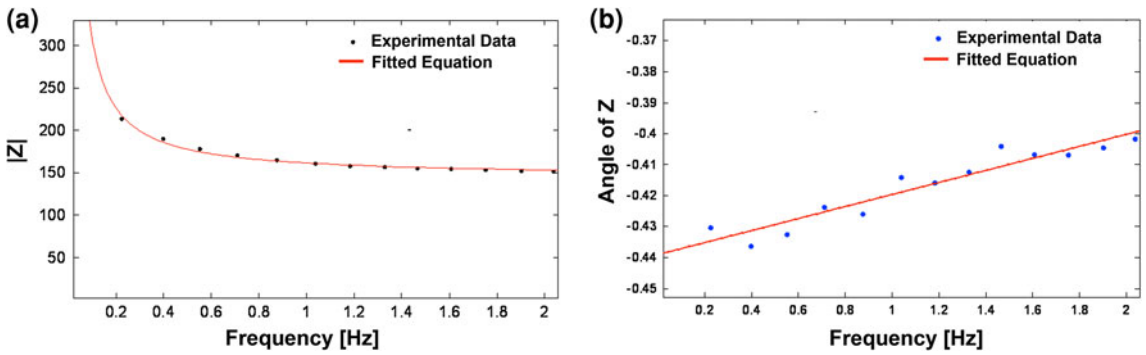

Fig. 5 Fit of the magnitude of the textile electrode impedance (**a**), Phase of the textile electrode impedance (**b**)

Table 3 Confusion matrix of QDC classifier for arousal level recognition

QDC	Feature set	N	A1	A2	A3	A4
N	α	**95.7 ± 3.9**	33.6 ± 18.7	33.6 ± 17.5	23.6 ± 16.2	20.7 ± 16.4
	β	**100 ± 0**	5.0 ± 8.4	5.0 ± 7	0 ± 0	3.6 ± 6.3
	γ	**100 ± 0**	10.0 ± 9.4	3.8 ± 2.1	5.3 ± 3.3	9.2 ± 12.5
A1	α	2.7 ± 3.8	**26.4 ± 22.8**	10.7 ± 13	5.7 ± 8.5	4.21 ± 1.4
	β	0 ± 0	**95.0 ± 8.4**	0 ± 0	0 ± 0	0 ± 0
	γ	0 ± 0	**90.0 ± 9.4**	0 ± 0	0 ± 0	0 ± 0
A2	α	0.9 ± 1.9	27.1 ± 13	**25.7 ± 22**	43.6 ± 26.4	30.7 ± 26.7
	β	0 ± 0	0 ± 0	**91.4 ± 9.7**	0 ± 0	0.7 ± 3.2
	γ	0 ± 0	0 ± 0	**96.2 ± 2.1**	0 ± 0	0 ± 0
A3	α	0.3 ± 1.1	3.6 ± 6.3	17.1 ± 15.8	**11.4 ± 9.9**	27.1 ± 18.5
	β	0 ± 0	0 ± 0	0 ± 0	**92 ± 10.8**	7.1 ± 10.9
	γ	0 ± 0	0 ± 0	0 ± 0	**94.7 ± 3.3**	1.6 ± 4.4
A4	α	0.3 ± 1.1	9.3 ± 16.9	12.8 ± 17.9	15.7 ± 19	**17.1 ± 20.5**
	β	0 ± 0	0 ± 0	3.6 ± 6.3	7.9 ± 10.8	**88.5 ± 12.8**
	γ	0 ± 0	0 ± 0	0 ± 0	0 **± 0**	**89.2 ± 13.8**

α Refers to the standard feature set when a PCA-reduction to 19 components is applied; β refers to the set of features extracted using non-linear methods, after applying a PCA method to reduce to seven components; γ refers to the set including both standard and non-linear methods-extracted features. All of the values reported in the table are expressed in terms of mean and standard deviation. The figures in bold emphasize the percentages ofthe correctly recognized classes

was extracted from the EDR and used as input to a classifier to recognize five arousal classes. Electrode characterization has been performed calculating the voltage–current characteristics as well as the electric impedance of the textile electrode and finding that the electric behavior is comparable with standard electrodes. In addition, we have designed and realized an acquisition protocol, where signals from textile and standard electrodes are simultaneously acquired, in order to verify if textile electrodes were suitable for EDR acquisition. The results have been very satisfactory and showed that textile electrodes can be used likewise standard electrodes without loss of information. A dedicated affective computing experiment was designed, where 35 healthy subjects wearing the glove were presented with sets of images gathered from IAPS. Rows α in Table 3 show how standard features, used alone, are able to recognize with an acceptable percentage only the neutral class, while is less effective for the other classes. Rows β show the percentages of recognition of each class that when features extracted from non-linear methods are used. Results are satisfactory and all the classes can be discriminated with a low error. Rows γ refer to the results obtained when both features extracted from standard and non-linear methods are used. It is worthwhile that the classifier is able to discriminate the classes with satisfactory percentages of successful recognition. Slightly higher performance can be achieved when the classifier uses the feature set γ. However, we can conclude that the contribution provided by the features extracted from non-linear methods is essential to attain much better results.

Nevertheless, to have more statistical significance the number of subjects could be increased. This problem is partially overtaken doing a cross validation in the classification process, i.e., randomizing the subjects for training and test set. It makes the classification independent from the sequence of the involved subjects. Results are very promising and open up new scenarios in the field of emotion recognition during activity. Indeed, a sensing glove allows us to investigate emotion fluctuations during naturalistic elicitation. Next works will aim at evaluating the movement artifact effect on the quality of the EDR acquired during dynamic tasks.

Acknowledgments This research is partially supported by the EU Commission under contracts FP7-ICT-247777 PSYCHE and FP7-ICT-258749 CEEDs.

References

1. Bradley MM, Lang PJ (2000) Affective reactions to acoustic stimuli. Psychophysiology 37(2):204–215
2. Brillinger DR, Rosenblatt M, Petropulu PM (1967) Computation and interpretation of kth order spectra. Spectral analysis of time series. Wiley, New York, pp 189–232
3. Chang TT Ng, Sun SF (2004) Blind detection of photomontage using higher order statistics. In: Proceedings of IEEE international symposium on circuits and systems (ISCAS), Vancouver, Canada
4. Christie IC, Friedman BH (2004) Autonomic specificity of discrete emotion and dimensions of affective space: a multivariate approach. Int J Psychophysiol 51(2):143–153
5. Chua KC, Chandran V, Acharya UR, Lim CM (2008) Cardiac state diagnosis using higher order spectra of heart rate variability. J Med Eng Technol 32(2):145–155

6. Damasio A (2005) Descartes error: emotion, reason, and the human brain. Putnam, USA
7. De Rossi D, Carpi F, Lorussi F, Mazzoldi A, Paradiso R, Scilingo EP, Tognetti A (2003) Electroactive fabrics and wearable biomonitoring devices. AUTEX Res J 3(4):180–185
8. Duda RO, Hart PE, Stork DG (2001) Pattern classification. Citeseer. Wiley, New York
9. Eckmann JP, Kamphorst SO, Ruelle D (1987) Recurrence plots of dynamical systems. Europhys Lett 4:973
10. Fowles DC, Christie MJ, Edelberg R, Grings WW, Lykken DT, Venables PH (1981) Publication recommendations for electrodermal measurements. Psychophysiology 18(3):232–239
11. Freedman LW, Scerbo AS, Dawson ME, Raine A, McClure WO, Venables PH (1994) The relationship of sweat gland count to electrodermal activity. Psychophysiology 31(2):196–200
12. Geddes LA (1997) Historical evolution of circuit models for the electrode-electrolyte interface. Ann Biomed Eng 25(1):1–14
13. Gomez P, Danuser B (2004) Affective and physiological responses to environmental noises and music. Int J Psychophysiol 53(2):91–103
14. Gratch J, Marsella S (2005) Evaluating a computational model of emotion. Auton Agent Multi Agent Syst 11(1):23–43
15. Heiman GW (1995) Research methods in psychology. Houghton-Mifflin Co., Boston
16. Ishchenko AN, Shev'ev PP (1989) Automated complex for multiparameter analysis of the galvanic skin response signal. Biomed Eng 23(3):113–117
17. Jain AK, Mao RPWJ (2000) Statistical pattern recognition: a review. IEEE Trans Pattern Anal Mach Intell 22(1):4–37
18. Jolliffe I (2002) Principal component analysis. Wiley Online Library
19. Kim J, André E (2008) Emotion recognition based on physiological changes in music listening. In: Proceedings of IEEE transactions on pattern analysis and machine intelligence, pp 2067–2083
20. Koelstra S, Yazdani A, Soleymani M, Mühl C, Lee JS, Nijholt A, Pun T, Ebrahimi T, Patras I (2010) Single trial classification of EEG and peripheral physiological signals for recognition of emotions induced by music videos. Brain Inf 6334:89–100
21. Lang P, Bradley M, Cuthbert B (2005) International affective picture system IAPS: Digitized photographs, instruction manual and affective ratings. Technical report A-6. University of Florida
22. Lang PJ, Greenwald MK, Bradley MM, Hamm AO (1993) Looking at pictures: affective, facial, visceral, and behavioral reactions. Psychophysiology 30(3):261–273
23. Marwan N, Carmen Romano M, Thiel M, Kurths J (2007) Recurrence plots for the analysis of complex systems. Phys Rep 438(5–6):237–329
24. McCurdy HG (1950) Consciousness and the galvanometer. Psychol Rev 57(6):322–327
25. Mendel JM (1991) Tutorial on higher-order statistics (spectra) in signal processing and system theory: theoretical results and some applications. Proc IEEE 79:278–305
26. Nasoz F, Alvarez K, Lisetti CL, Finkelstein N (2003) Emotion recognition from physiological signals for presence technologies. Int J Cognit Technol Work-Special Issue Presence 6(1)
27. Nikias CL (1993) Higher-order spectral analysis: a nonlinear signal processing framework. PTR Prentice-Hall Inc., USA
28. Onaral B, Schwan HP (1982) Linear and nonlinear properties of platinum electrode polarisation. Part 1: frequency dependence at very low frequencies. Med Biol Eng Compu 20(3):299–306
29. Peng CK, Havlin S, Stanley HE, Goldberger AL (1995) Quantification of scaling exponents and crossover phenomena in nonstationary heartbeat time series. Chaos Interdiscip J Nonlin Sci 5(1):82
30. Picard RW, Vyzas E, Healey J (2001) Toward machine emotional intelligence: Analysis of affective physiological state. In: Proceedings of IEEE transactions on pattern analysis and machine intelligence 1175–1191
31. Pollak V (1974) Computation of the impedance characteristic of metal electrodes for biological investigations. Med Biol Eng Compu 12(4):460–464
32. Posner J, Russell JA, Peterson BS (2005) The circumplex model of affect: an integrative approach to affective neuroscience, cognitive development, and psychopathology. Dev Psychopathol 17(03):715–734
33. Russell JA (1980) A circumplex model of affect. J Pers Soc Psychol 39(6):1161–1178
34. Sabatinelli D, Lang PJ, Keil A, Bradley MM (2007) Emotional perception: correlation of functional MRI and event-related potentials. Cereb Cortex 17(5):1085
35. Schinkel S, Dimigen O, Marwan N (2008) Selection of recurrence threshold for signal detection. Eur Phys J Special Topics 164(1):45–53
36. Scilingo EP, Gemignani A, Paradiso R, Taccini N, Ghelarducci B, De Rossi D (2005) Performance evaluation of sensing fabrics for monitoring physiological and biomechanical variables. IEEE Trans Inf Technol Biomed 9(3):345–352
37. Venables PH, Christie MJ (1980) Electrodermal activity. In: Martins I, Venables PH (eds) Techniques in psychophysiology. Wiley, New York, pp 3–67
38. Wagner J, Kim J, André E (2005) From physiological signals to emotions: Implementing and comparing selected methods for feature extraction and classification. In: Proceedings of the IEEE international conference on multimedia and expo, pp 940–943
39. Winton WM, Wutnam LE, Krauss RM (1984) Facial and autonomic manifestations of the dimensional structure of emotion. J Exp Soc Psychol 20(3):195–216
40. Zbilut JP, Webber Jr CL (2006) Recurrence quantification analysis. Wiley Online Library